Fluctuations, commensurability, and structures found in Monte Carlo simulations of finite one-dimensional chains on a periodic substrate

Allison S. Hartnett and James M. Phillips
Department of Physics, University of Missouri-Kansas City, Kansas City, Missouri 64110, USA
(Received 6 July 2007; revised manuscript received 27 September 2007; published 8 January 2008)

Finite one-dimensional chains adsorbed on a periodic potential were simulated using a hybrid isobaric ensemble. Our simulations are unique because we observe structures forbidden in macroscopic systems. Density fluctuations dominate the system and produce a mixture of coexisting thermodynamic structures. Stable structures were rare. We applied a lattice gas approximation to the observed fragmentations in the chains with success. Our goal was to test these systems for experimentally measurable changes in enthalpy. Chains fragment into clusters having nearly the same size, which contrasts with the size distributions found in three-dimensional vapors.

DOI: 10.1103/PhysRevB.77.035408 PACS number(s): 65.80.+n, 64.60.−i, 05.20.−y, 05.10.Ln

I. INTRODUCTION

Experimental and theoretical studies of one-dimensional systems have recently shown[1–12] the value of numerous older theoretical investigations[13–21] in the history of one-dimensional statistical mechanics. The flowering of nanotechnology has revived an interest in the detailed behavior of one-dimensional models for finite clusters of atoms and molecules.[5,22–24] Phillips and Dash[25] have recently shown that many of the traditional understandings about one-dimensional systems are valid in finite sized simulations but some new properties are observed. They found that the ordering of clusters occurs if the system is short and cold. The dynamics of the clusters were driven by fluctuations which caused disordering at chain end points. At higher temperatures fragmentation of the chains occurs.

We seek to extend our investigation by considering a finite chain interacting with a periodic adsorption potential and we test the system for experimentally observable properties. The differences in the simulations in this paper from the earlier work[25] are the unique hybrid method of using a pressure ensemble on a fixed substrate potential and the resulting structures that occur in the form of commensurability, light and heavy walls, and free floating clusters. Both studies show fragmentation of the clusters in a manner different from three-dimensional vapors.

In Sec. II, we discuss the thermodynamics of small systems. Section III defines the interactions we used for the computations. Section IV explains our simulation methodology. We present the lattice gas model in Sec. V. In Sec. VI, we report our results on the thermodynamic structures found in our model. Sections. VII and VIII report our simulation results obtained from the 100 and 300 particle systems, respectively. Our conclusions are given in Sec. IX. The Appendix demonstrates that our hybrid ensemble generates Markov chains.

II. THERMODYNAMICS OF FINITE ONE-DIMENSIONAL CHAINS

Our computations are for small systems using an isobaric ensemble with (N,p,T) as the environmental variables. A single small system, by definition, is not in the thermodynamic limit and in one dimension, we do not have phases. We observe a mix of unique thermodynamic structures.

The experiments we have in mind are one-dimensional versions of the traditional heat capacity studies of two-dimensional adsorbates on solid surfaces such as physical adsorption on the surface of bundles of single walled nanotubes.[1–12] Other possibilities could be molecular chains that have been adsorbed on channels or steps often found on metal substrates. In the case of one-dimensional zeolites, their quasi-one-dimensional character in some cases could exceed the restricted geometry used in our simulations but the lattice gas model would certainly be applicable.[26–28] Our model should be useful in a general way because we use reduced variables which can be scaled using corresponding state theory. Hence, our model represents a wide category of systems. These experiments are carried out with precise changes in the temperature and the chemical potential is accomplished by controlling the three-dimensional vapor pressure which is in equilibrium contact with adsorbate. Hence, the pressure and the temperature must be included in the thermodynamic variables used in our simulations.

It was shown in the previous work by Phillips and Dash[25] that thermal fluctuations drive the structural configuration in the one-dimensional system and that the size of the cluster is the limiting factor for the magnitude of the enthalpy available within the individual cluster to undergoing structural change. Consequently, we use the number of particles in the cluster to be the final thermodynamic variable completing the set of independent variables in our simulations (NpT). In the following, we show how the formalism is structured in our approach and how it justifies our generated ensemble averages. Our simulated results will be slightly different from those that would be taken using a macroscopic system but our ensemble averages are the ones that should be compared with experiment under the same conditions.

Our model requires the ensemble to be $\aleph$ chains of N molecules each. This system is closed to additional particles but in contact with temperature and pressure reservoirs.[29–31] If $\aleph \to \infty$, then the ensemble is a macroscopic thermodynamic system. A single small chain is one element in the larger ensemble. Our computations are for the internal properties of

the single finite chain. The entire collection of the generated configurations provides us with the ensemble averages for the finite chain.

Following the notation of Hill,[29]

$$dE_t = TdS_t - pdV_t + \mu\aleph dN + Xd\aleph, \tag{1}$$

where

$$X \equiv \left(\frac{\partial E_t}{\partial \aleph}\right)_{S_t,V_t,N} = \hat{\mu}N \tag{2}$$

and $S_t=\aleph S$ and $V_t=\aleph\bar{V}$. The subscript t refers to averages over the entire ensemble. The bar over a variable represents the average value for the small system. The variable $\hat{\mu}$ is the integral chemical potential per particle representing molecules being added to the ensemble in groups of N and μ is the differential chemical potential per particle representing the work done in adding a single particle to each of the chains in the ensemble. In the macroscopic limit, we have $\mu=\hat{\mu}$. However, in small finite systems they are not equal. The combined law written for a small system is

$$d[N(\hat{\mu}-\mu)] = d\Gamma = -SdT + \bar{V}dp + \mu dN, \tag{3}$$

where Γ is a measure of the Gibbs free energy difference due to the finite nature of the system. This difference is generally small when applied to linear chains for $N \geqslant 100$. We monitor the enthalpy for the small system in our isobaric ensemble simulations. Thermodynamically, this is written as

$$H = \bar{E} + p\bar{V}. \tag{4}$$

The environmental pressure p from the (NpT) ensemble is the same pressure in the small system. An experimental observation of fragmentations and structural changes in a finite chain is an open question. We have sought to estimate the changes in the heat capacity that accompany these structural differences. A heat capacity measurement involves the possibility of observing

$$C_p = \left(\frac{\partial H}{\partial T}\right)_{N,p} = \frac{\overline{H^2} - \bar{H}^2}{kT^2}. \tag{5}$$

In terms of statistical mechanics

$$\hat{\mu} = -\frac{kT}{N}\ln \Delta(N,p,T) \tag{6}$$

with

$$\Delta(N,p,T) = \sum_V \Omega(N,V,T)e^{-pV/kT} = \sum_V Q(N,V,T)e^{-pV/kT}, \tag{7}$$

where $Q(N,V,T)$ is the canonical partition function. In our one-dimensional simulations, we use $\bar{V} \equiv \bar{L}$.

In a previous study,[25] Phillips and Dash demonstrated that it was the density fluctuations which drove the system to end point disordering or fragmentation of the finite linear chain. In the present work, we also find the chain fragmentation an important effect. The probability of fluctuations in the density of a certain size to be

$$P(n)dn = (2\pi\sigma_0)^{-1/2}e^{-(n-n_{av})^2/2\sigma_0^2}dn \tag{8}$$

with the density dispersion

$$(n-n_{av})^2 = n_{av}^2(kT/BL). \tag{9}$$

The dimensionless bulk modulus is $B\bar{L}/kT$. If the density fluctuation is large enough and the small chain contains sufficient energy, then the chain will fragment. In the earlier paper of Phillips and Dash,[25] we searched for the conditions when this fragmentation occurs on a smooth substrate. In this paper we sought the same information when the adsorbate is in a periodic adsorption potential. For example, conditions for commensurability with the substrate and for the formation of walled structures or free floating clusters are forbidden in the thermodynamic limit.[32] The thermodynamic limit of the one-dimensional model with a finite wall energy will have no commensurate phase and consequently no commensurate-incommensurate transition.[33] As we demonstrate, small systems are quite different from that of the conventional wisdom for macroscopic one-dimensional models interacting with a periodic potential.

III. MODELS

We have chosen a finite linear chain of Lennard-Jones interacting particles on a sinusoidal external potential whose amplitude is adjustable. To better approximate an experimental system in contact with a supplied vapor pressure, we selected a (NpT) ensemble for our simulations. The internal potential energy for a finite chain is

$$u_{in} = \sum_{i<j}^{N} 4\varepsilon\left[\left(\frac{\sigma}{x_{ij}}\right)^{12} - \left(\frac{\sigma}{x_{ij}}\right)^{6}\right]. \tag{10}$$

The potential for a system of particles at given locations on the corrugation is given by

$$u_{ext} = \sum_{i=1}^{N} \frac{1}{2}\omega\varepsilon\left[1 - \cos\left(\frac{2\pi x_i}{a}\right)\right], \tag{11}$$

where a is the periodicity of the substrate. The amplitude of the corrugation is $(\frac{1}{2})\omega\varepsilon$. The ω is an adjustable factor on the depth of the corrugation. The LJ(12,6) potential allows us to cover a broad range of possible systems through the theory of corresponding states.

We assumed the wavelength for the corrugation to be $a=1.1279$, which is the nearest neighbor distance for a chain with $T \to 0$ and with zero pressure on a flat substrate. We chose this periodicity in order to have a ground state match between the adsorbate and the substrate. At the start of a computation, the system is initialized to be in a registered configuration. In this manner, we were able to observe the effects of temperature and pressure on a chain by using various amplitudes for the corrugation.

IV. SIMULATIONS

We have used a hybrid version to the Monte Carlo approach in the simulation of an isobaric (NpT) ensemble and

we have elected to use reduced variables for distance $x^* = R/\sigma$ and temperature $t^* = kT/\varepsilon$, where σ and ε are the LJ parameters. The reduced pressure is $p^* = p\sigma/\varepsilon$ and the reduced amplitude is $\omega^* = \omega/\varepsilon$. To simulate an isobaric ensemble, one rescales the positions of the particles to a larger and/or smaller length in order to approach the given pressure. A problem arises when one has a fixed external potential as in our sinusoidal potential. Note that the external potential does not rescale. We attempt to solve this problem by requiring the rescaling to be limited to a small adjustment factor and then running additional cycles as a canonical ensemble to allow the particles to relax to the fixed corrugation. These additional *NVT* cycles are not included in the ensemble averages. The dual application of both of these Monte Carlo approaches will generate a converging Markov chain provided the rescale factor is kept quite small relative to the wavelength of the corrugation.[34] We used one-tenth σ for this factor. Further details are provided in the Appendix.

Using this algorithm, we compute the ensemble averages for the dimensionless enthalpy

$$H/NkT, \tag{12}$$

and the misfit of the chain relative to the substrate corrugation,

$$m = \frac{b-a}{a}. \tag{13}$$

In Eq. (13), the length b is the thermal average of the intermolecular separation and the factor a is the fixed distance for the minimum to minimum length in the corrugation.

We also monitor the graphic constructions for every 1000 Monte Carlo steps as a snapshot of the configuration. Our ensemble averages are over 100 000 Monte Carlo moves per particle or 10×10^6 averaging configurations for the $N=100$ simulations

V. APPLICATION OF THE ONE-DIMENSIONAL LATTICE GAS MODEL TO CHAIN FRAGMENTATION

A very simple but reasonably accurate model is found in Hill Refs. 30 and 31 using a one-dimensional lattice gas to study adsorption. In this model, there are M equivalent linear adsorption sites for N molecules. The molecules have only nearest neighbor interactions. When two molecules are occupying adjacent sites, they have w potential energy. The partition function for a single isolated molecule on a site is $q(T)$. In a given configuration, there are N_{11} nearest neighbor pairs and N_{01} pairs where one site is empty. The canonical partition function for this ensemble is

$$Q(N,M\ .\ T) = q^N \sum_{N_{01}} g(N,M,N_{01}) \exp\left[-\left(N - \frac{N_{01}}{2}\right)\frac{w}{kT}\right],$$

which simplifies to

$$Q(N,M\ .\ T) = (qe^{-w/kT})^N \sum_{N_{01}} g(N,M,N_{01})(e^{w/2kT})^{N_{01}}, \tag{14}$$

where the sum is over all possible values of N_{01} for a given N and M. Applying the maximum term method[35] to the combinatorial factor $g(N,M,N_{01})$ will produce $\hat{N}_{01}$ by solving

$$e^{-w/kT} = \frac{\left(\frac{N}{M} - \frac{\hat{N}_{01}}{2M}\right)}{\left(\frac{\hat{N}_{01}}{2M}\right)^2}. \tag{15}$$

We define $\hat{N}_{01}$ to be the value of the maximum term found by solving Eq. (15). Our calculation for $\hat{N}_{01}$ will give the number of end points to the continuous clusters observed in the linear chain with a known N and M.

TABLE I. The number of clusters $C(t^*)$ observed in Ref. 25 compared to the solution to Eq. (15) for a system of 100 molecules. Note, the number of clusters is one half the number of end points $\hat{N}_{01}$.

$t^* = \frac{kT}{\varepsilon}$	$C(t^*)$	$\hat{N}_{01}$
0.02	6	12.0
0.04	5	10.0
0.06	4	8.0
0.08	3	6.0

It is interesting to evaluate this approximation from the data found in Ref. 25 for a system with no corrugation potential. In this paper,[25] the simulation starts with a dilute chain of separated molecules and the system is then allowed to relax to form continuous clusters. The limiting cluster size was observed for four temperatures. These results and the solutions to Eq. (15) for $\hat{N}_{01}$ are shown in Table I. It appears that a lattice gas model predicts the cluster size quite well for our simple system of 100 particles and no corrugation. As we show in the following sections, the comparison is also reasonable for simulations where the sinusoidal corrugation is included.

VI. SIMULATIONS OF THE ONE-DIMENSIONAL LJ(12,6) CHAIN MODEL WITH A SINUSOIDAL ADSORPTION POTENTIAL

Using the model described in Sec. III, we computed the properties of the *NpT* ensemble for a variety of temperatures and for a number of amplitudes for the adsorption potential. Our purpose in simulating this matrix of computations is to predict the possible conditions that have a chance of showing measurable results in thermodynamic experiments. For example, can we find a set of conditions that show an enthalpy change large enough to be measurable in heat capacity experiments? One of the most serious problems in these calculations is the rarity of conditions that produce a stable thermodynamic structure. A consequence of this set of rare conditions is that monitoring the difference found in the thermal properties between two different stable structures presents a difficult experimental problem. As we show in the next section, only some of the conditions yield registered (commensurate) structures that are stable. However, we find

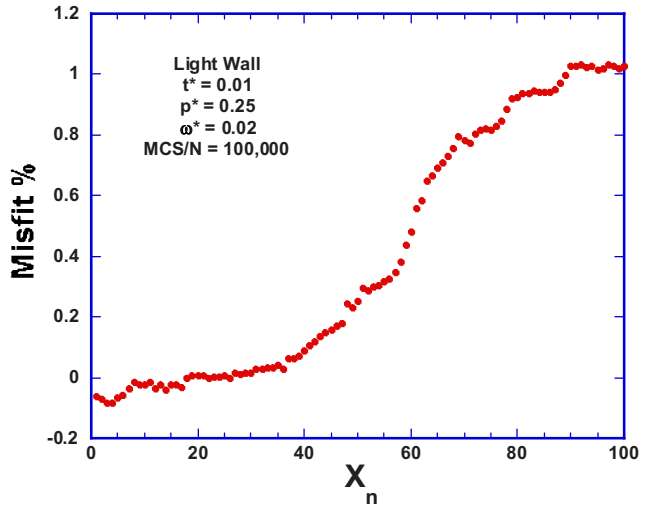

FIG. 1. (Color online) A snapshot of the particle locations expanded relative to the substrate minima (light wall) which remained stable for 100 000 Monte Carlo steps per particle (MCS/N). There are 100 particles expanded over 101 substrate wells. The reduced temperature is $t^*=0.01$, the reduced pressure is $p^*=0.25$, and the amplitude for corrugation is $\omega^*=0.02$.

a number of fragmented clusters to be quite stable when the temperature is sufficiently high. Under many conditions, the chain does not converge to a fixed structure but the system is driven by the fluctuations to form a mix of coexisting configurations. As examples of the mix of structures we observe those shown in Figs. 1–5. These snapshots show the different types of structures found in the chain of 100 particles. We have named them as follows: light walls (Fig. 1), registered (Fig. 2), heavy walls (Fig. 3), free floating (Fig. 4), and fragmented (Fig. 5). Fragmented structures converge to reasonably stable configurations.

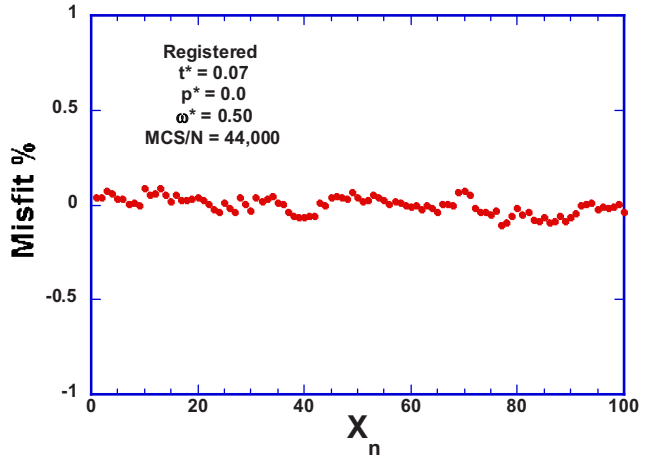

FIG. 2. (Color online) A momentary snapshot of the system in a commensurate (registered) configuration. This is one of a structural mix of coexisting configurations for these same conditions. The reduced temperature is $t^*=0.07$, the reduced pressure is $p^*=0.0$, and the amplitude for corrugation is $\omega^*=0.50$. This particular configuration was observed at 44 000 MSC/N.

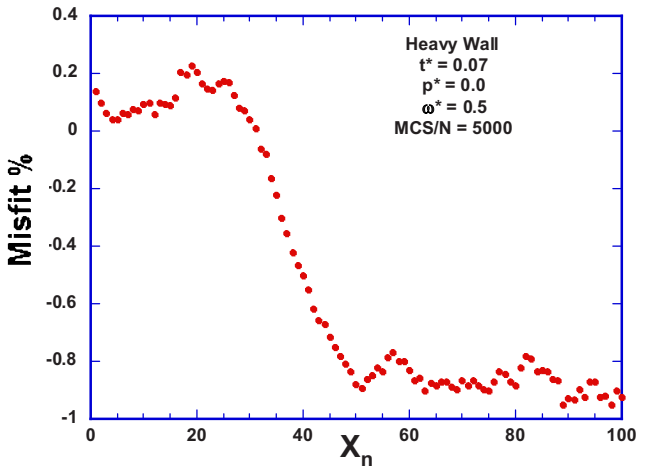

FIG. 3. (Color online) A momentary snapshot of the particle locations compressed relative to the substrate minima (heavy wall) at 5000 MCS/N in a 100 000 MSC/N run. This is one of a mix of structures coexisting for these same conditions. There are 100 particles spread over 99 substrate wells. The reduced temperature is $t^*=0.07$, the reduced pressure is $p^*=0.0$, and the amplitude for corrugation is $\omega^*=0.50$.

VII. RESULTS FOR A CHAIN WITH 100 PARTICLES

We report only two series of pressure scans for the corrugation amplitudes $\omega^*=0.02$ with $t^*=0.03$ and $t^*=0.04$ in Figs. 6 and 7. These scans are quite typical. In the dimensionless enthalpy and misfit plots shown in Fig. 6, the first two points are off the trend from the rest of the results be-

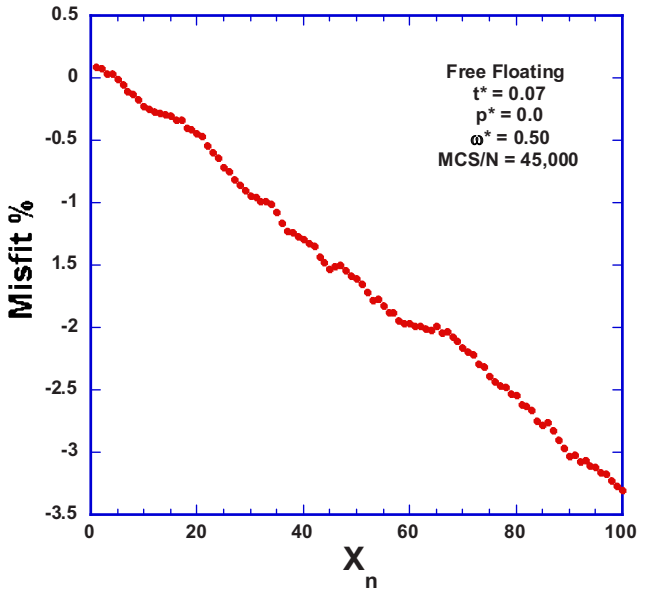

FIG. 4. (Color online) A momentary snapshot of the particle locations relative to the substrate minima (free floating) in a mix of coexisting configurations occurring after 45 000 MCS/N in a 100 000 MCS/N run. There are 100 particles expanded over 103 substrate wells. The chain does not conform to the corrugations. The reduced temperature is $t^*=0.07$, the reduced pressure is $p^*=0.0$, and the amplitude for corrugation is $\omega^*=0.50$.

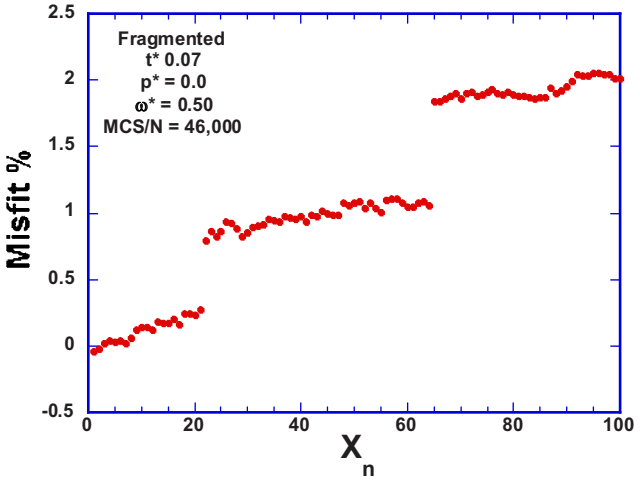

FIG. 5. (Color online) A snapshot of the particle locations relative to the substrate minima which show a fragmentation of the chain. There are 100 particles expanded over 102 substrate wells. The reduced temperature is $t^*=0.07$, the reduced pressure is $p^*=0.0$, and the amplitude for corrugation is $\omega^*=0.50$. The clusters appeared to be stable after 46 000 MSC/N for the rest of the 100 000 MSC/N run.

cause the amplitude is low and the chain is fragmented. In this case, the pressures $p^*=0.0$ and 0.1 have allowed the chain to break up. The third point, $p^*=0.2$, is a mix of light walls, registered, and heavy walls. This typical mix continues until $p^*=0.60$ where the free floating structure is added to the mix and the light wall structures are no longer observed. The mix of the other structures continues until the $p^*=2.8$. Beyond this, the pressure is great enough that the chain becomes free floating and does not conform to the corrugation. The misfit in the last two points shows that the

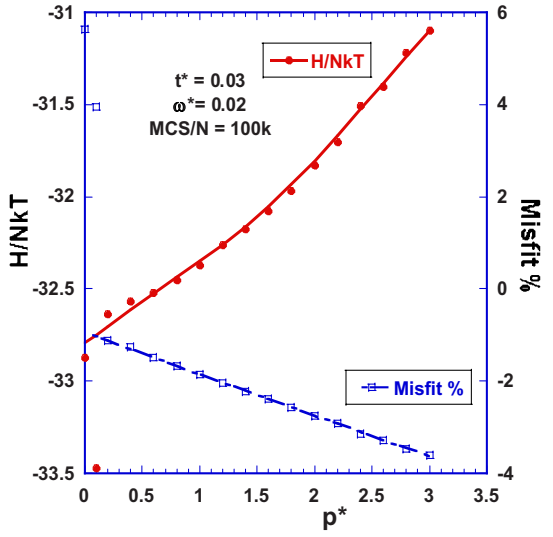

FIG. 6. (Color online) A plot of a pressure scan for the dimensionless enthalpy (left axis) and the misfit (right axis). The conditions are reduced temperature $t^*=0.03$ and reduced amplitude $\omega^*=0.02$. Each point represents an average over a 100 000 MCS/N. Lines are a weighted fit as a guide to the eyes.

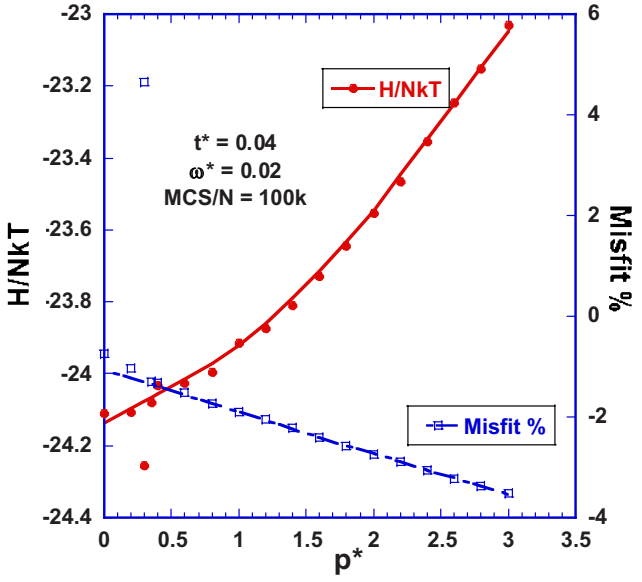

FIG. 7. (Color online) A plot of a pressure scan for the dimensionless enthalpy (left axis) and the misfit (right axis). The conditions are reduced temperature $t^*=0.04$ and reduced amplitude $\omega^*=0.02$. Lines are a weighted fit as a guide to the eyes. Each point represents an average over a 100 000 MCS/N.

chain of 100 particles is compressed into 96 substrate corrugations.

In Fig. 7, we plot the enthalpy and misfit for a series of simulations with varying pressure for a fixed $t^*=0.04$ and the amplitude $\omega^*=0.02$. With this slightly higher temperature, the fragmentations appear until $p^*=0.035$. A mix of structures is present up to $p^*=3.0$ where the pressure forces the chain to be free floating.

Figure 8 plots the enthalpy and misfit where the amplitude $\omega^*=0.3$ is deeper and the temperature $t^*=0.03$ as in Fig. 6. The chain is registered at the lower pressures $p^*=0.1$ and 0.2. In the pressure range $p^*=0.3-4.4$, the chain is a volatile mix of the structures. With the higher amplitude, larger fluctuations are needed to change from one structure to another. When $p^*=4.5$ the fluctuations cannot overcome the corrugation and the system is in a stable registered configuration. This is one of the few simulations where we found a single structure throughout the computation. In the three highest pressures $p^*=4.6$, 4.7, and 4.8 the stress supplied by the pressure is dominate. These structures are all free floating. This range of pressures could be difficult to achieve experimentally.

Using a different cut through the "phase diagram," we show how the enthalpy of the system varies with the reduced temperature as shown in Fig. 9. This would roughly demonstrate the path taken by an experiment measuring heat capacity. We try to approximate the conditions for a heat capacity measurement with the $p^*=0.0$ and for a deep amplitude $\omega^*=0.50$. The first three points $t^*=0.01$, 0.02, and 0.03 in Fig. 9 are held in registry by the corrugation. In the temperature range $t^*=0.04-0.0625$, the system is a mixture of structures. Above $t^*=0.0625$, the system begins to fragment into clusters. As an example of a path taken by the system evolving into a final fragmentation, we show this structure in three

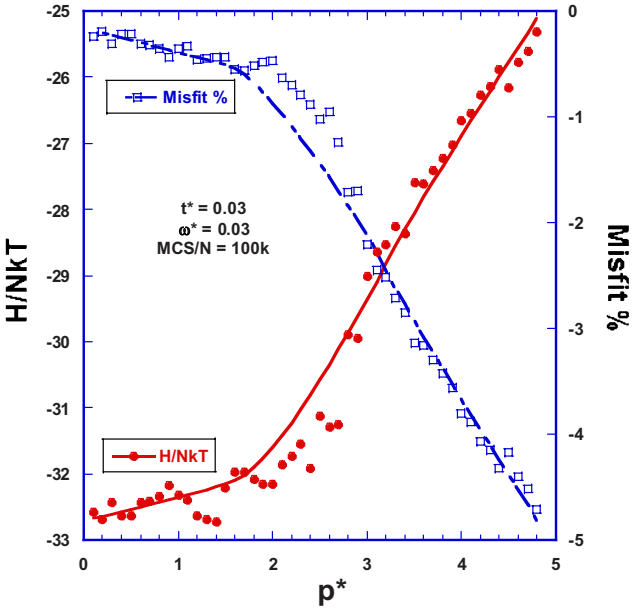

FIG. 8. (Color online) A plot of a pressure scan for the dimensionless enthalpy (left axis) and the misfit (right axis). The conditions are reduced temperature $t^*=0.03$ and reduced amplitude $\omega^*=0.3$. Each point represents an average over a 100 000 MCS/N. Each point represents an average over a 100 000 MCS/N. The lines are a weighted fit as a guide to the eyes.

snapshots of progressing configurations (see Fig. 10).

Since the fragmentation of a chain is a likely candidate for experimental observation, we have summarized our results in

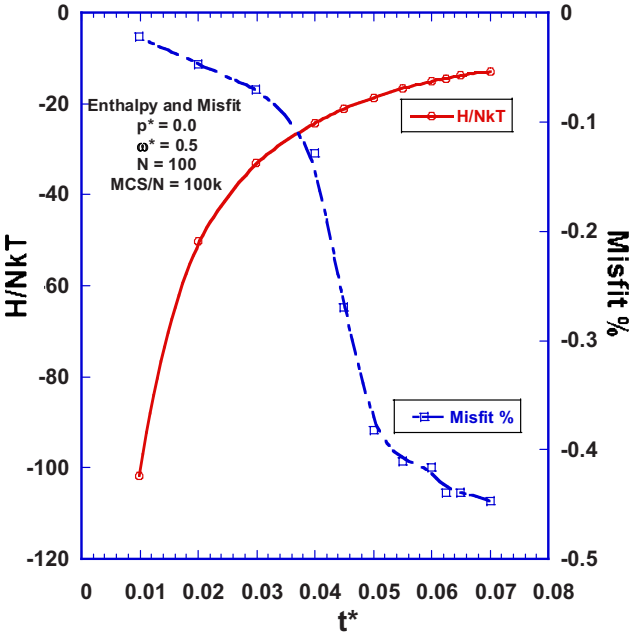

FIG. 9. (Color online) A plot of a temperature scan from $t^*=0.01$ to 0.07, with $p^*=0.0$, and the amplitude $\omega^*=0.5$ for the dimensionless enthalpy (left axis) and the misfit (right axis). Each point represents an average over a 100 000 MCS/N. The lines are a weighted fit as a guide to the eyes.

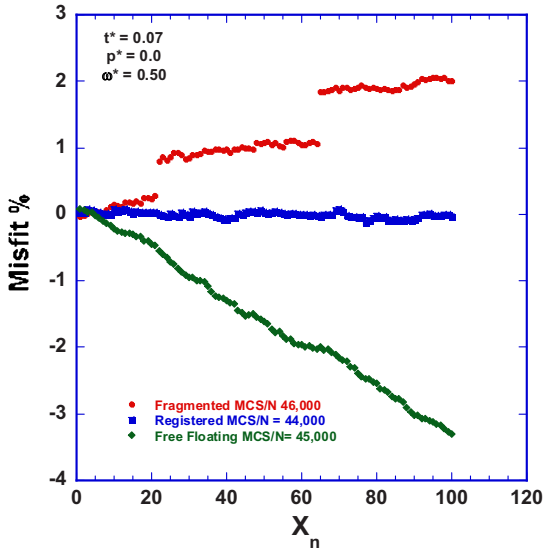

FIG. 10. (Color online) A depiction of three snapshots of the particle locations as the system moves from a registered structure, to a free floating configuration, and then to a stable fragmented chain. The temperature $t^*=0.07$, the pressure $p^*=0.0$, and the corrugation amplitude $\omega^*=0.5$.

Table II. We compare the calculated fragmentation predictions using the lattice gas model with our observations. To do this, we have added the amplitude of the corrugation into the w found in Eq. (15). The lattice gas approximation is a reasonable fit to the lattice gas model with $N=100$ for a chain adsorbed onto a corrugation both conceptually and computationally.

VIII. RESULTS FOR A CHAIN WITH 300 PARTICLES

We increased the number of particles in the chain to illustrate some of the effects that chain length has on the resulting structures. A longer chain has more total energy and consequently the fluctuations will have a greater upper limit. Many of the configurations for the 100 particle system are also observable in the longer chain simulations but additional fea-

TABLE II. The number of clusters $C(t^*)$ for two separate corrugated amplitudes ω^*, each with 100 molecules. The number of clusters will be nearly twice the number of $\hat{N}_{01}$ end points from Eq. (15). The error is calculated between $2C(t^*)$ and $\hat{N}_{01}$.

ω^*	$t^*=\frac{kT}{\varepsilon}$	$p^*=\frac{p\sigma}{\varepsilon}$	$C(t^*)$	$\hat{N}_{01}$	Error (%)
0.020	0.03	0.0	6	11.38995	5.08
0.020	0.03	0.1	3	5.83487	2.75
0.020	0.03	0.2	3	5.83487	2.75
0.020	0.20	0.2	2	3.92453	1.89
0.020	0.20	0.2125	2	3.92453	1.89
0.500	0.07	0.0	3	5.95916	0.68
0.500	0.65	0.0	2	3.97042	0.74

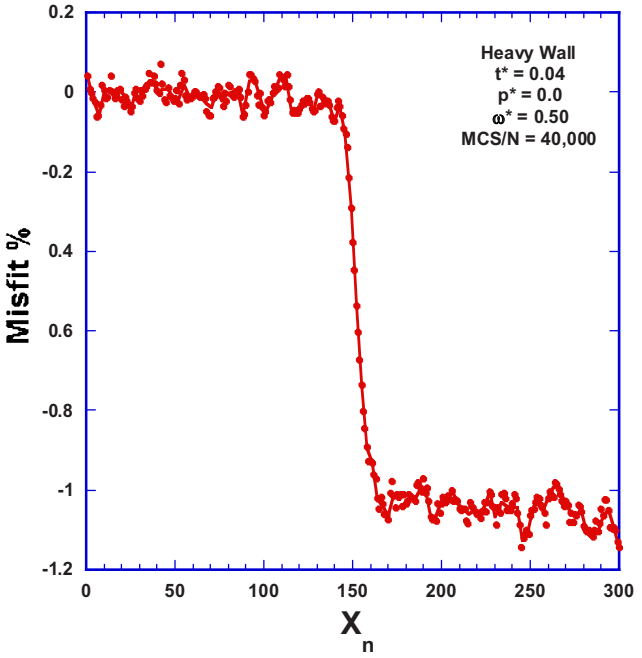

FIG. 11. (Color online) A snapshot of a stable heavy wall structure for a system with $N=300$, $t^*=0.03$, $p^*=0.0$, and $\omega^*=0.50$. The enthalpy difference in this heavy wall structure when compared to a commensurate chain under these conditions is less by $\Delta H/NkT=0.746$.

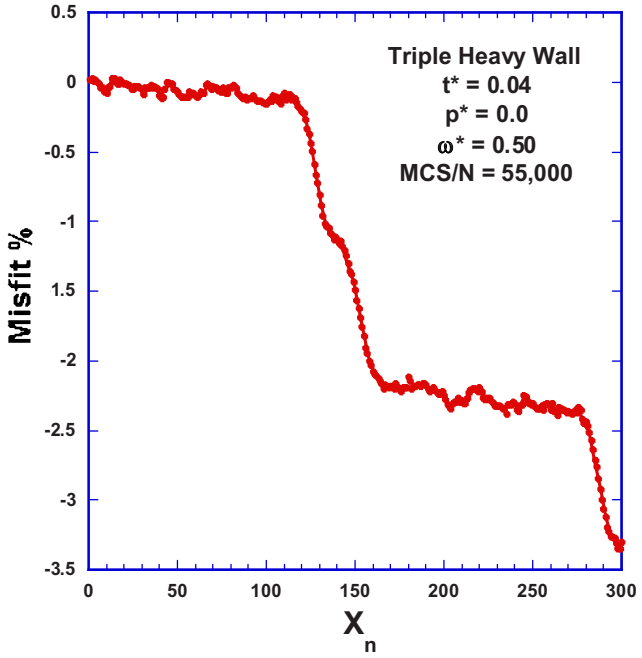

FIG. 12. (Color online) A momentary snapshot of an intermediate structure of a triple heavy wall taken at 55 000 MCS/N with $t^*=0.04$, $p^*=0.0$, and amplitude $\omega^*=0.5$. This structure eventually evolves into a stable fragmented chain.

tures are also present. We shall present some examples of these structures. In Fig. 11, the heavy wall structure occurs for a system with $N=300$, $t^*=0.03$, $p^*=0.0$, and $\omega^*=0.5$. The wall length is similar to that in the shorter chain, but in this case the heavy wall, once formed, is quite stable due to the higher amplitude. A heavy wall is a compressed structure like those shown in Figs. 3 and 11. Under the conditions in Fig. 11, the system allows us to monitor the dimensionless enthalpy of a stable registered chain for over half of the run. Continuing this run, the final structure result is stable heavy wall. The enthalpy difference in forming the heavy wall from a commensurate chain is less by $\Delta H/NkT=0.746$. This may indicate that a heat capacity measurement is possible provided experimental problems can be overcome.

Figure 12 is an intermediate structure of three heavy walls with $t^*=0.04$, $p^*=0.0$, and amplitude $\omega^*=0.5$. This structure evolves into a stable fragmented chain. This chain of 300 particles is compressed to reside over 297 potential wells of the corrugation before fragmentation.

Figure 13 compares the pressure effects on the enthalpy when run is over identical scans for the temperature while the amplitude remains the same, $\omega^*=0.5$. The pressures in these simulations were fixed at $p^*=0.0$, 0.02, and 0.03. In the temperature range $t^*=0.01-0.03$, all of the chains are registered. At higher temperatures, all of these scans were eventually fragmented. Figure 14 is plot of the chain with $t^*=0.10$, $p^*=0.0$, and $\omega^*=0.5$ resulting in ten clusters.

A summary of these fragmentations compared with the lattice gas predictions is shown in Table III. Since the fragmentation for a longer chain is more probable, one could expect fragmentations to be a property more easily observed experimentally. Our calculated fragmentation predictions used the lattice gas model with the amplitude of the corrugation added into w as before in the 100 particle system (Table II). The results in Table III are from computations

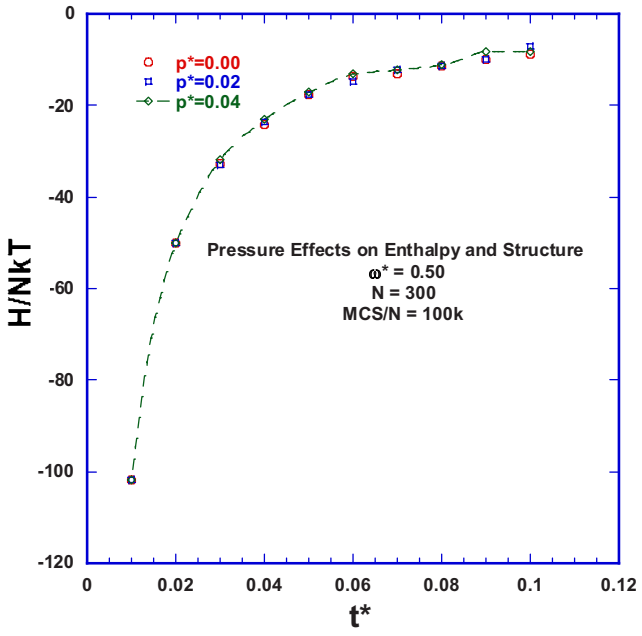

FIG. 13. (Color online) A plot of the dimensionless enthalpy over three pressure scans ($p^*=0.0$, 0.02, and 0.03) with changing temperature and the amplitude $\omega^*=0.5$. In the temperature range $t^*=0.01-0.03$ the chains are stable and registered. At the two highest temperatures, all of these scans were fragmented.

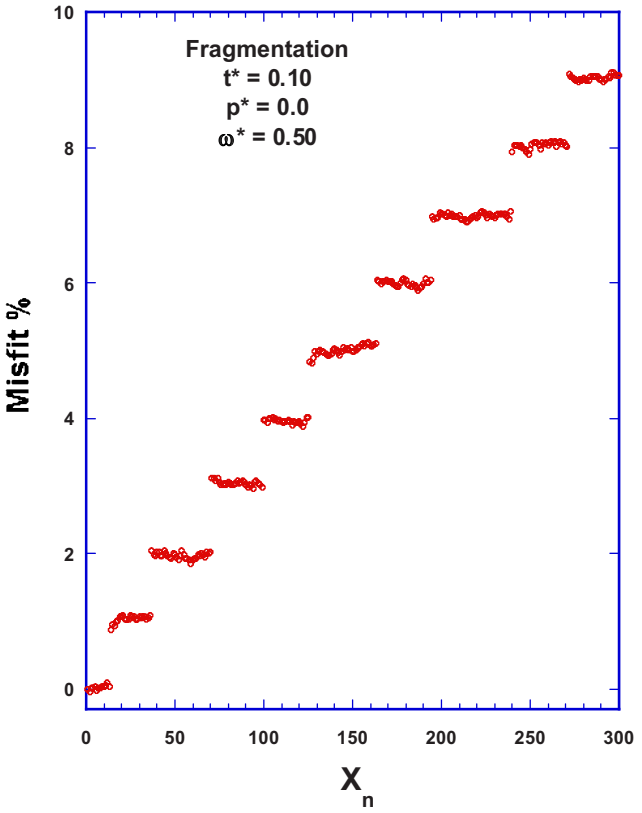

FIG. 14. (Color online) A snapshot of a stable chain of 300 particles with $t^*=0.10$, $p^*=0.0$, and $\omega^*=0.5$ resulting in ten fragments. MCS/N=100 000.

using a deeper amplitude for the corrugation. They appear to be closer to the lattice gas model than those in Table II. This should be the case because the larger corrugation is a better comparison to the lattice gas approximation.

IX. CONCLUSIONS

We simulated finite one-dimensional clusters adsorbed on a periodic potential. Our observations show that density fluctuations dominate in these systems and produce a variety of coexisting thermodynamic structures. Only a few conditions appear to result in stable structures. Stable chain structures tend to be located in regions of low temperature, low pressure, or else in high amplitude models in the corrugation. The most common stable structures are fragmentations found at higher temperatures and lower pressures with systems having deep minima in the periodic substrate. Our results show that large fluctuations drive the system to fragment into smaller clusters. Once a chain is fragmented, the resulting clusters appear to be stable. The lattice gas approximation we used for the flat substrate is nearly as precise as in the cases with corrugation and gives a reasonable prediction for the number of stable clusters (see Tables II and III).

Small changes in the amplitude of the corrugation or small change in temperature have small changes in structural and thermodynamic properties. When the conditions are such that a wall formation or a fragmentation is eminent, the small increase beyond the threshold will show a mark system response (see Figs. 6 and 7). Figures 9 and 13 show the small changes in enthalpy with gradual temperature increases even when fragmentation has begun.

We were concerned about these effects being observable experimentally. First, the chain lengths would need to be close to the same size in a physical sample. In Ref. 25 it was demonstrated that cluster sizes, for a set temperature, disordered at the end points until the chains are of the same approximate length. An array of one-dimensional clusters in a given sample could well be taken as an ensemble with $\aleph$ chains of N molecules in a closed system with respect to additional particles.[29]

The second question to be considered is whether the changes in enthalpy of the system with increasing temperature would be sizable enough to be measurable [see Eq. (5)]: In Fig. 11, we reported the change in enthalpy as a registered structure became a heavy wall configuration. In this case, the drop in dimensionless enthalpy was found to be 0.746 for a single chain which for an ensemble containing $\aleph$ chains could well be measurable.

Possibly a more achievable system would be an ensemble $\aleph$ of registered long chains taken to a fragmentation temperature. In such a system (see Fig. 14), the change in enthalpy would be a measure of the creation of the number of free ends. Since this type of structural change is more common than the isolation of rare configurations of other stable structures in the mix, it could provide a possible experimental goal. An approximation of these systems with a lattice gas type of calculation would be a useful tool in search for a

TABLE III. The number of clusters $C(t^*)$ for corrugated amplitudes $\omega^*=\omega/\varepsilon$, with 300 molecules. The number of clusters should be nearly twice the number of end points $\hat{N}_{01}$ from Eq. (15).

ω^*	$t^*=\frac{kT}{\varepsilon}$	$p^*=\frac{p\sigma}{\varepsilon}$	$C(t^*)$	$\hat{N}_{01}$	Error
0.50	0.06	0.02	15	29.999	0.00
0.50	0.06	0.04	18	35.999	0.00
0.50	0.07	0.02	17	33.999	0.00
0.50	0.07	0.04	16	31.999	0.00
0.50	0.08	0.00	4	7.985	0.18
0.50	0.08	0.02	17	33.999	0.00
0.50	0.09	0.00	6	11.987	0.10

fruitful combination of adsorbate and substrate candidates.

Our principle contributions to the subject of one-dimensional chains of particles are in our observing structures and effects for finite systems that would be forbidden in macroscopic chains. Advances in nanotechnology have been developed to the extent that experiments could now be carried out on samples where the chain length is in the range of small system thermodynamics. We have attempted to simulate models which exhibit behaviors that are not predicted in the long chains of macroscopic dimension. In particular, one expects a macroscopic model with finite wall energy to have no commensurate phase at nonzero temperatures.[32,33] In such a case, there could be no commensurate-incommensurate transitions. Simple arguments exist for refuting the possibility of an ordered low-temperature phase for a one-dimensional chain of pairwise interacting particles in a zero substrate potential.

In our simulations, we do not have phases nor transitions in the traditional sense but we do have ordered and disordered thermodynamic structures and changes between them. Our prediction is that these structural changes have the possibility of being observable in heat capacity measurements. We find adsorbates with light and heavy wall structures. There are conditions that produce commensurate adsorbates and we also found conditions where the system is free floating, thus incommensurate. We offer the lattice gas model for locating the conditions which cause fragmentations.

Undoubtedly, testing our simulations with experiment will be difficult. It is our hope that these simulations would be a helpful guide in a design of such an experiment.

It is important to note that a small chain has an upper limit to its energy. A finite source of energy in the chain will place an upper bound on the magnitude of the fluctuations that are allowed to occur in the chain. As we observed, fragments will converge to a size where the energy required to further fragment the chain is unavailable within the cluster. Once a system fragments, the residual clusters will be nearly the same size. Rather than a system breaking up into clusters of random length, the fragmentation process generates clusters of a similar size. This is noteworthy because in three-dimensional vapor, physical clusters form a distribution of sizes as one approaches a three-dimensional vapor condensation limit.[35] We do not observe any cases where clusters form a size distribution in a small one-dimensional chain.

ACKNOWLEDGMENTS

We thank J. G. Dash for his continued interest and advice in our discussions of low dimensional models and David Thouless for his suggestions in use of lattice models.

APPENDIX

Our simulations use a hybrid Monte Carlo approach which is primarily an isobaric (NpT) ensemble where each step is followed by a rescaling of the particle positions. A further random relaxation of each particle over the fixed periodic potential is accomplished before returning to the pressure simulation steps. The dual algorithm allows the system to converge by generating a Markov chain of energy relaxations between the steps of another Markov chain which rescales the computational cell to match the required pressure. This convergence is achieved provided that the relaxation steps are limited in size to a small constant value.

Initially, the pressure ensemble simulation generates a new length for the chain, L_{new}. This is then compared with the existing length, L_{old}. We require $|L_{\text{new}}-L_{\text{old}}|<\delta_L$, for a chosen small step size δ_L. The chain length is changed to converge to the given pressure, consequently, the position of the particles must also be scaled proportionally. To achieve this, a set of intermediate relaxation steps for the particle positions is required.

If we define x_i^p as the original position of the ith particle in the chain during a step in the NpT ensemble and $x_i'^p$ as the corresponding atom's position after rescaling, then $x_i'^p=(L_{\text{new}}/L_{\text{old}})x_i^p$ for each particle. After these position adjustments are complete, the program begins a canonical Monte Carlo relaxation (NVT) which adjusts each of the particles to the fixed periodic potential for the same L_{new}. The purpose of the dual ensembles is to allow the chain to achieve convergence over the fixed potential. To start the relaxation, we compute the total energy for the chain, U_{new}. Then we compute the change in energy, ΔU where $\Delta U=U_{\text{new}}-U_{\text{old}}$. If $\Delta U\leqslant 0$, then the system will accept the new positions U_{new}. However, if $\Delta U>0$ then the algorithm will accept U_{new} after a comparison between the Boltzmann factor for this energy and a random number. The newly random number is between 0 and 1 and defined as R_C. Then U_{new} will be accepted if $e^{-\Delta U/kT}\geqslant R_C$. In the event that $e^{-\Delta U/kT}<R_C$, U_{new} is rejected. After the rescaling and the relaxation, we return to the calculation for convergence in pressure ΔP for the next cycle. The change in enthalpy ΔH in the NpT system is computed for its contribution to the ensemble average.

The routine for the pressure ensemble is very similar to that in the canonical ensemble, with one notable exception that comparison in the Boltzmann factor uses the enthalpy rather than the internal energy. If the change in enthalpy is negative, we accept L_{new}. In the case where the change in enthalpy is positive, the algorithm then computes the factor $e^{-\Delta H/kT}$. A new random number R_p is created (again between 0 and 1). If $e^{-\Delta H/kT}\geqslant R_P$ then accept L_{new}. However, if $e^{-\Delta H/kT}<R_P$, then L_{new} is rejected. The pressure ensemble continues in this fashion until the preset number of Monte Carlo steps occurs.

In order to verify that our hybrid algorithm constitutes a Markov process, we need to show that the probability of a step depends only on the immediate previous state. Consider events X_{old} and X_{new} that correspond to states S_{old} and S_{new}. Given information about the old state, we want the probability that event X_{new} is in state S_{new}. The probability for such a stochastic process is written as $P(X_{\text{new}}=S_{\text{new}}|X_{\text{old}}=S_{\text{old}})$.[36] The hallmark of this process is that only information about the previous configuration is required[37,38] to predict the outcome of future events.

In the relaxation process, each new energy U_{new} is a state for that particular step. Specifically, $P(X_{\text{new}}=S_{\text{new}}|X_{\text{old}}=S_{\text{old}})$ which determines the probability for the acceptance of $X_{\text{new}}=U_{\text{old}}$. A similar correlation can be found for the pres-

sure ensemble where the Boltzmann factor uses the enthalpy rather than the internal energy difference in predicting the next step. Each successive step, in both aspects of the simulation, is a change (be it in length or energy) which depends on the previous state. The absence of information about the previous $(n-2)$ and the following $(n+1)$ steps do not enter into the determination of successive operations. Furthermore, between successive steps in the pressure ensemble we have $|\Delta P| < \delta_P$ which allows the process to be convergent.

[1] S. Talapatra, S. E. Weber, C. Journet, D. Zambrano, and A. D. Migone, Phys. Rev. B **61**, 13150 (2000).
[2] S. Talapatra, A. Zambano, S. E. Weber, and A. D. Migone, Phys. Rev. Lett. **85**, 138 (2000).
[3] S. Talapatra and A. D. Migone, Phys. Rev. Lett. **87**, 206106 (2001).
[4] M. Muris, N. Dufau, M. Bienfait, N. Dupont-Pavlovshy, Y. Grillet, and J. P. Palmari, Langmuir **16**, 7018 (2000).
[5] L. W. Bruch and R. Kariotis, Phys. Rev. B **73**, 193404 (2006).
[6] D. Cao and J. Wu, Langmuir **20**, 3759 (2004).
[7] T. Wilson and O. E. Vilches, Low Temp. Phys. **29**, 732 (2003).
[8] J. V. Pearce, M. A. Adams, O. E. Vilches, M. R. Johnson, and H. R. Glyde, Phys. Rev. Lett. **95**, 185302 (2005).
[9] N. Bendiab, R. Almairac, S. Rols, R. Aznar, J. L. Sauvajol, and I. Mirebeau, Phys. Rev. B **69**, 195415 (2004).
[10] J. Cambedouzou, S. Rols, N. Bendiab, R. Almairac, J. L. Sauvajol, P. Petit, C. Mathis, I. Mirebeau, and M. Johnson, Phys. Rev. B **72**, 041404 (2005).
[11] Liang Chen and J. Karl Johnson, Phys. Rev. Lett. **94**, 125701 (2005).
[12] P. Puech, E. Flahaut, A. Sapelkin, H. Hubel, D. J. Dunstan, G. Landa, and W. S. Bacsa, Phys. Rev. B **73**, 233408 (2006).
[13] John A. Barker, Aust. J. Phys. **15**, 127 (1962).
[14] Elliot H. Lieb and Daniel C. Mattis, *Mathematical Physics in One Dimension: Exactly Soluble Models of Interacting Particles* (Academic, New York, 1966).
[15] Daniel C. Mattis, *The Many-Body Problem: An Encyclopedia of Exactly Solved Models in One-Dimension* (World Scientific, River Edge, NJ, 1993).
[16] Marvin Bishop and Martin Boonstra, Am. J. Phys. **51**, 564 (1983).
[17] L. van Hove, Physica **16**, 137 (1950).
[18] R. Peierls, J. Phys. Chem. A **5**, 177 (1935).
[19] Zevi W. Salsburg, Peter J. Wojtowicz, and John G. Kirkwood, J. Chem. Phys. **26**, 1533 (1957).
[20] H. Takahashi, Proc. Phys. Math. Soc. Jpn. **24**, 60 (1942).
[21] Lewi Tonks, Phys. Rev. **50**, 955 (1936).
[22] M. M. Calbi, S. M. Gatica, M. J. Bojan, and M. W. Cole, J. Chem. Phys. **115**, 9975 (2001).
[23] M. K. Kostov, M. M. Calbi, and M. W. Cole, Phys. Rev. B **68**, 245403 (2003).
[24] M. Q. Zhang, J. Phys. A **24**, 3949 (1991).
[25] James M. Phillips and J. G. Dash, J. Stat. Phys. **120**, 721 (2005).
[26] Michael Springborg, J. Solid State Chem. **176**, 311 (2003).
[27] R. Radhakrishnan and Keith E. Gubbins, Phys. Rev. Lett. **79**, 2847 (1997).
[28] Patricia Enzel and Thomas Bein, J. Phys. Chem. **93**, 6270 (1989).
[29] Terrell L. Hill, J. Chem. Phys. **36**, 3182 (1962).
[30] Terrell L. Hill, *Thermodynamics of Small Systems: Part I and II* (W. A. Benjamin, New York, 1963).
[31] Terrell L. Hill, *Introduction to Statistical Thermodynamics* (Addison-Wesley, Reading, MA, 1960).
[32] P. Bak, Rep. Prog. Phys. **45**, 587 (1982).
[33] M. E. Fisher and D. S. Fisher, Phys. Rev. B **25**, 3192 (1982).
[34] Dan Wang (unpublished).
[35] Terrell L. Hill, *Statistical Mechanics: Principles and Selected Applications* (McGraw Hill, New York, 1956).
[36] Bernd Berg, *Markov Chain Monte Carlo Simulations and Their Statistical Analysis: With Web-Based Fortran Code* (World Scientific, Hackensack, NJ, 2004).
[37] W. S. Kendall, F. Liang, and J.-S. Wang, *Lecture Note Series: Institute for Mathematical Sciences, National University of Singapore*, edited by Louis H. Y. Chen and Denny Leung (World Scientific, Singapore, 2005), Vol. 7.
[38] Richard L. Scheaffer, *Introduction to Probability and its Applications* (Duxbury Press, Belmont, CA, 1995).